ACERP: Vol. 3, No. 1, (Winter 2017) 1-5

Advanced Ceramics Progress

Research Article

Journal Homepage: www.acerp.ir

# Evaluation of Microstructure and Mechanical Properties of Bulk Nanostructured $Ti_5Si_3$ and $Ti_5Si_3$-$Al_2O_3$ Nanocomposites

S. Sabooni*, F. Karimzadeh, M.H. Abbasi, M.H. Enayati

*Department of Materials Engineering, Isfahan University of Technology, Isfahan, Iran*

*PAPER INFO*

*Paper history:*
Received 14 November 2016
Accepted in revised form 06 May 2017

*Keywords*:
Intermetallics matrix composite
Mechanical alloying
Fracture toughness
Nanoindentation
Powder processing

*ABSTRACT*

Mechanical alloying and pressure less sintering in vacuum have been used to produce bulk nanostructured $Ti_5Si_3$ and $Ti_5Si_3$-15wt.% $Al_2O_3$ nanocomposite. X-Ray Diffraction (XRD), Scanning Electron Microscopy (SEM) and Transmission Electron Microscopy (TEM) were used to study the microstructural characteristics of the samples. Indentation method was used to calculate hardness, elastic modulus and fracture toughness of bulk samples. The results showed that the nanometric grains were obtained through mechanical alloying and remained in nanometric scale after subsequent sintering. It was also observed that the in-situ produced $Al_2O_3$ through mechanochemical reaction has amorphous structure which was crystallized during sintering process. Nanohardness, elastic modulus and fracture toughness of $Ti_5Si_3$-15wt.% $Al_2O_3$ nanocomposite were calculated as 1660 HV, 238 GPa and 5.5 MPa.$m^{1/2}$ ,respectively, that are higher than those of the monolithic $Ti_5Si_3$. Toughening mechanisms based on crack deflection and crack bridging were suggested as responsible factors for fracture toughness increase of the $Ti_5Si_3/Al_2O_3$ nanocomposite.

## 1. INTRODUCTION

Development of intermetallic compounds is due to the needs for structural materials with better characteristics and performance, especially at high temperatures [1-2]. Intermetallic compounds have been the focus of significant investigations during the past decades. Among the intermetallics, silicide compounds have many desirable properties such as high melting point, relatively low density, and high corrosion, wear and creep resistance. In the recent years, refractory metal silicides such as $Ti_5Si_3$ have attracted much interest among various kinds of silicides. Monolithic Ti5Si3 has been successfully fabricated by various methods such as arc melting [3], Shock assisted synthesis [4], self-propagating high temperature synthesis (SHS) [5], etc. Limitations such as poor ductility and toughness (2.5 MPa.m1/2) are serious problems which should be overcome in monolithic $Ti_5Si_3$. Grain size reduction and addition of second phase particles are known as the most promising approaches to increase fracture toughness of structural intermetallic compounds. Li et al. [6] studied the microstructure and mechanical properties of $Ti_5Si_3$-TiC nanocomposite and reported improvement of room temperature ductility and high temperature strength. However, not much improvement was observed in the fracture toughness of bulk nanostructured $Ti_5Si_3$ produced by Counihan et al. [7] which was related to existence of oxygen and nitrogen contamination in the powders. Compatibility between reinforcement particles and matrix and uniform distribution of reinforcements are also important issues in composite forming. In-situ synthesis of reinforcement phase in the matrix has advantage over other synthesis routes due to its capability to produce chemical compatible phase as well as nanosized structure with high uniformity [8]. So, the aim of the present study was to synthesize and characterize bulk nanostructured $Ti_5Si_3$ and bulk $Ti_5Si_3$-15wt.% Al2O3 nanocomposite by mechanochemical reaction and sintering and comparison of their microstructure and mechanical properties.

*Corresponding Author's Email: s.sabooni@ma.iut.ac.ir (S.Sabooni)

## 2. MATERIALS AND METHODS

High purity Ti, Si, Al and $TiO_2$ were used as initial powders. Ti-26wt.% Si was milled to synthesize nanostructured $Ti_5Si_3$. To produce in-situ $Ti_5Si_3$-15wt.% $Al_2O_3$ nanocomposite, a mixture of Ti-18$TiO_2$-22Si-8Al (wt.%) powders were used. Mechanical alloying was performed at room temperature under Ar atmosphere. In all mechanical alloying (MA) runs, the ball to powder weight ratio and rotational speed were 10:1 and 500 rpm, respectively. After 60h of milling, mechanically

alloyed powders were cold pressed in a 6mm die at a pressure of 700 MPa and sintered in a vacuum furnace at 1400 $^0$C for 90 min to obtain bulk nanostructured composites. The structural features of powder particles and consolidated samples were studied by X-Ray diffraction, scanning electron microscope (Philips XL30) and transmission electron microscope (Philips EM208s). Image analysis software was used to calculate the average grain size of $Ti_5Si_3$ powders from TEM image. The crystallite size of powder particles and the compacted samples was calculated using Williamson-Hall formula [9]:

$$\beta_{sample} \cos\theta = (0.9\,\lambda/D) + 2\,\varepsilon \sin\theta \quad (1)$$

where D is the average grain size, θ is the diffraction angle, ε is the internal strain, λ is the used X-Ray wavelength, and $\beta_{sample}$ is the full width at half maximum intensity (FWHM). For instrumental correction, Gaussian-Gaussian relation was used:

$$\beta_{sample}^2 = \beta_{exp}^2 - \beta_{ins}^2 \quad (2)$$

where $\beta_{ins}$ is the FWHM of the annealed powder and $\beta_{exp}$ is the measured FWHM. The value of average strain can be estimated from the linear slope of $\beta_{sample}\cos\theta$ versus $2\sin\theta$, while the average crystallite size can be estimated from the intersection of this line at $\sin\theta = 0$. Mechanical properties of the consolidated samples were also evaluated using indentation methods. Vickers micro-indentation was carried out using a Buehler microhardness tester with a load of 100 gr. Nanoindentation tests were also performed using a nanoindentation tester (NHTX S/N: 01-03119, CSM Instrument) with a Berkovich indenter tip under the scan rate of 10 nm/sec. Indentations were performed on the surface of bulk samples. Small size of bulk samples guarantees the uniformity of microstructure and mechanical properties throughout different areas. The following equations were used to calculate nanohardness and elastic modulus of bulk samples according to Olivier-Pharr method [10]. The contact depth $h_c$ was calculated from Eq. (3):

$$h_c = h_m - \varepsilon\,(F_m/S) \quad (3)$$

where $h_m$ is the maximum penetration depth, $F_m$ is the maximum force in the nanoindentation test (30mN) and S is the stiffness of unloading curve (S= dF/dh). The instrumented hardness $H_{IT}$ is determined using Eq. (4).

$$H_{IT} = (F_m/A_p) \quad (4)$$

where $A_p$ is the cross section area.
The Vickers hardness HV was then calculated using the developed area ($A_d$):

$$HV = (F_m/A_d) \quad (5)$$

Reduced modulus, $E_{IT}^*$, was used because of the fact that the elastic displacement occurs both in the indenter and the sample. $E_{IT}^*$ can be calculated using Eq. 6:

$$E_{IT}^* = \frac{\sqrt{\pi}}{2}\frac{S}{\sqrt{A_p}} \quad (6)$$

The instrumented elastic modulus, $E_{IT}$, was determined using the following equation:

$$E_{IT} = \frac{(1-\nu^2)}{\frac{1}{E_{IT}^*} - \frac{(1-\nu_i^2)}{E_i}} \quad (7)$$

In this equation, υ is the poison ratio for the sample, $E_i$ and $\upsilon_i$ are the elastic modulus and poison ratio of the indenter, respectively. The elastic constants $E_i$=1141 GPa and $\upsilon_i$=0.07 are used for a diamond indenter. It should be noted that nanoindentation tests were repeated for 5 times in different areas of the sample and the average results were reported.
The indentation fracture toughness of bulk samples was evaluated using the Evans formula [6].

$$K_{IC} = P\,(\pi\,c)^{-1.5}\,\mathrm{Cot}\,\beta \quad (8)$$

where P is the applied load, β is the Vickers indenter angle ($68^0$) and 2C is the crack length. At least five measurements were carried out and the average was reported as fracture toughness.

## 3. RESULT AND DISCUSSION

Fig. 1 shows the XRD patterns of $Ti_{62.5}Si_{37.5}$ (Ti-26 wt.% Si) powder mixture after different milling times. As shown, nanostructured $Ti_5Si_3$ intermetallic compounds (JCPDS card no 008-0041) from precursor powders was formed in a gradual mode. The average crystallite size of $Ti_5Si_3$ after 45 h of MA was found as 15 nm. Based on thermodynamic calculations which are presented in our previous study [11], formation of intermetallic compounds at the nominal composition of $Ti_5Si_3$ ($X_{si}$ = 0.375) has the lowest Gibbs free energy compared to solid solution or amorphous phases. The results of XRD are in accordance with the thermodynamic calculations and show that the intermetallic phase is stable during MA.

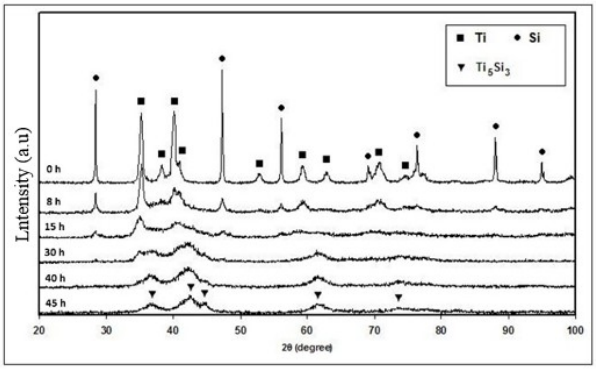


**Figure 1.** XRD patterns of $Ti_{62.5}Si_{37.5}$ powder mixture as – received and after different milling times.

The TEM image of nanostructured $Ti_5Si_3$ after 60h of milling and its related selected area diffraction (SAD) pattern are presented in Fig. 2. Selected Area Diffraction (SAD) pattern reveals that the microstructure is amorphous/nanocrystalline. Nanometric grains with the average grain size of 80 nm are clearly visible in the TEM image.

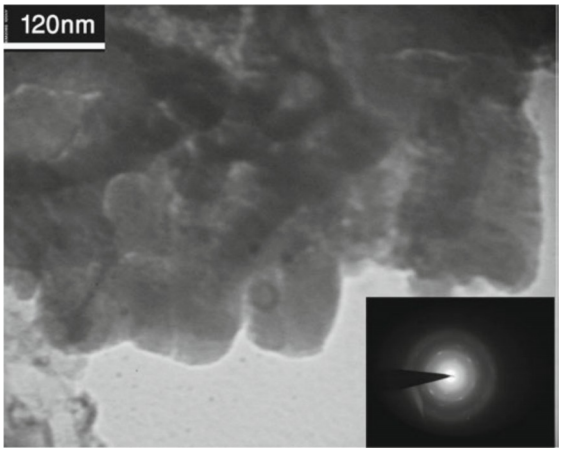


**Figure 2.** TEM micrograph of the nanostructured $Ti_5Si_3$ intermetallic compounds after 60 h of MA.

Fig. 3 shows the XRD patterns of $Ti_5Si_3$-15wt.% $Al_2O_3$ nanocomposite after 60h of MA and subsequent sintering. The XRD pattern of the nanocomposite after 60h of MA includes only $Ti_5Si_3$ peaks and no sign of $Al_2O_3$ was detected at this stage. This could be due to the amorphous nature of the produced $Al_2O_3$ or its nanometric size. It has been reported that the gradual proceeding of reduction process during MA sustains relatively low temperature which favors the formation of amorphous alumina. Meanwhile, the heat generated from the sudden formation of products in a combustion reduction can crystallize the produced $Al_2O_3$ [12-13]. After sintering process, the amorphous $Al_2O_3$ was crystallized and its related peaks can be clearly observed in the XRD pattern. The crystallite size of $Ti_5Si_3$-15wt.% $Al_2O_3$ nanocomposite after MA and subsequent sintering was calculated about 21 and 68 nm, respectively. As can be seen the average grain size of the produced composite after sintering is still in the nanometric region which confirms the positive effect of second phase particles incorporation to slow down grain growth. Second-phase particles act as obstacles to the motion of grain boundaries and thus retard grain growth based on the Zener pinning effect. With the migration of matrix grain boundaries toward center of their curvature during grain growth, the inclusions or second phase particles exert opposite restraining force on the boundaries. The effectiveness of pinning effect of second phase particles in the composite materials was previously reported [14-16].

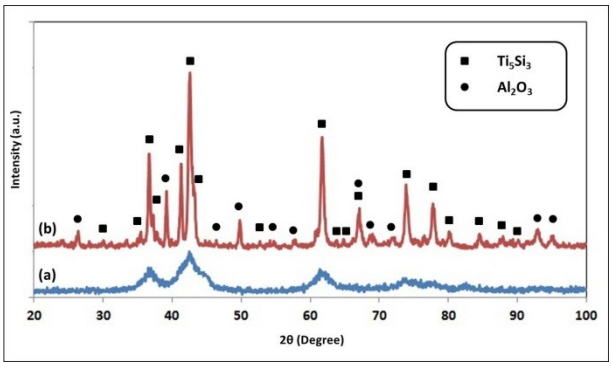


**Figure 3.** XRD patterns of $Ti_5Si_3$-15wt.% $Al_2O_3$ after (a) 60h of MA, and (b) sintering at 1400°C for 90min.

Cross sectional SEM image and related elemental map of sintered $Ti_5Si_3$-15wt.% $Al_2O_3$ nanocomposite are shown in Fig. 4. The dark points in the SEM image are remaining porosities after sintering process. The remaining porosity, measured by Archimedes method, was around 5%. Fine distribution of Al and O in the matrix can be inferred from the elemental map of the sample.

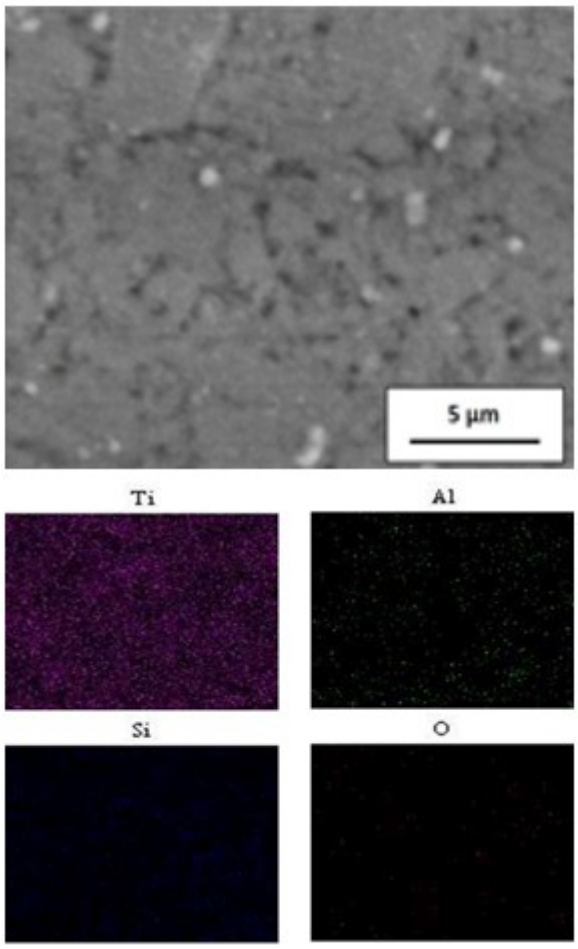


**Figure 4.** SEM micrograph and related elemental maps of sintered $Ti_5Si_3$-15Wt.% $Al_2O_3$ nanocomposite.

Fig. 5 shows the load- displacement curves of the bulk nanostructured $Ti_5Si_3$ and $Ti_5Si_3$-15wt.% $Al_2O_3$ nanocomposite. The differences between hardness of the samples can be obviously determined from their penetration depths. The nanohardness of the $Ti_5Si_3$ and $Ti_5Si_3$-$Al_2O_3$ nanocomposite was calculated as 1534 $\pm$ 120 and 1660 $\pm$ 150 HV. Meanwhile, the reported hardness values for $Ti_5Si_3$ intermetallic compounds in the literature vary too much which might be due to the grain size of the synthesized $Ti_5Si_3$. Rosenkranz [17] reported hardness of 968HV for $Ti_5Si_3$ produced by reaction sintering and hot pressing. However, Cheon et al., [18] reported hardness of about 1180 HV for electro discharge sintered $Ti_5Si_3$. In the present study, the higher obtained hardness is attributed to the lower crystallite size of nanostructured $Ti_5Si_3$. The elastic modulus of the $Ti_5Si_3$–$Al_2O_3$ nanocomposite (238 GPa) is also higher than that of the $Ti_5Si_3$ (187 GPa).

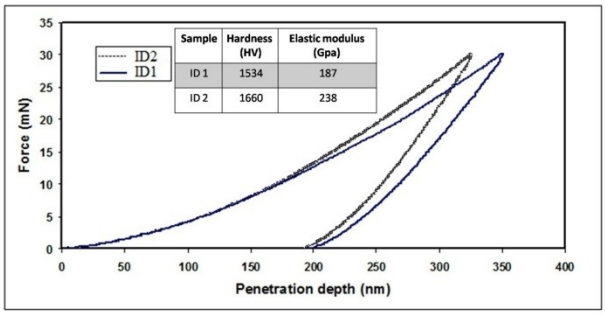


**Figure 5.** Nanoindentation load- displacement curves of the bulk nanostructured $Ti_5Si_3$ (ID 1), and $Ti_5Si_3$-15wt.% $Al_2O_3$ nanocomposite (ID 2).

The Vickers indentation fracture test is a unique experimental technique to estimate fracture toughness of brittle materials. The indentation methods are quick and easy to perform, require small samples and are applicable for special microstructural features [19]. This technique can estimate the fracture toughness of brittle materials using direct measuring of the crack length after indentation. Fig. 6 (a) shows the typical example of cracks extension in the $Ti_5Si_3$-15wt.% $Al_2O_3$ nanocomposite. The fracture toughness of nanostructured $Ti_5Si_3$ and $Ti_5Si_3$-15wt.% $Al_2O_3$ nanocomposite were calculated as about 4 and 5.5 $MPa.m^{1/2}$, respectively. Table 1 shows the fracture toughness of $Ti_5Si_3$ and $Ti_5Si_3$-based nanocomposites of this work and the similar samples which are reported in references.

The effect of grain size on the fracture toughness of brittle ceramics and intermetallic compounds has been previously studied. Rice et al., [20] reported that although dependence of fracture toughness on grain size of dense sintered body with non-cubic crystal structures was significant, the dense polycrystalline bodies with cubic crystal structure showed no significant dependence of fracture toughness on grain size. With respect to the hexagonal crystal structure of $Ti_5Si_3$, decrease of grain size could affect the fracture toughness of this material significantly. Nanostructured $Ti_5Si_3$ synthesized in this work showed fracture toughness increase by the order of 2 compared to the coarse $Ti_5Si_3$.

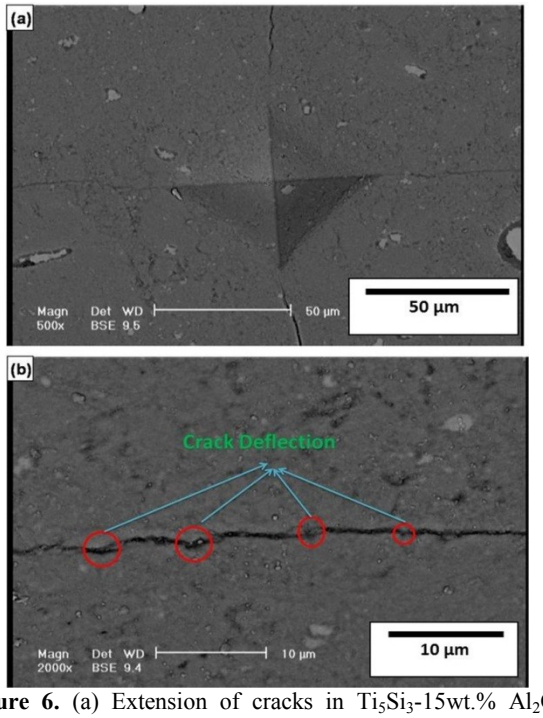


**Figure 6.** (a) Extension of cracks in $Ti_5Si_3$-15wt.% $Al_2O_3$ nanocomposite, and (b) Crack deflection as a mechanism for fracture toughness increase in $Ti_5Si_3$-$Al_2O_3$ nanocomposite.

**TABLE 1.** Fracture toughness of $Ti_5Si_3$ and $Ti_5Si_3$-based nanocomposites of this work and references.

| Composition | Fracture toughness ($Mpa.m^{1/2}$) | Synthesis method | Reference |
|---|---|---|---|
| $Ti_5Si_3$ (grain size: 50-150 nm) | 2-3 | Dynamic densification of amorphous Ti-Si powder | [7] |
| Nanostructured $Ti_5Si_3$ | 4 | Mechanical alloying | This work |
| $Ti_5Si_3$-14Vol.%TiC | 3 ± 0.2 | Hot reaction pressing | [6] |
| $Ti_5Si_3$-35Vol.%TiC | 4.2 ± 0.2 | Hot reaction pressing | [6] |
| $Ti_5Si_3$- 15Wt.% $Al_2O_3$ | 5.5 ± 0.5 | Mechanical alloying | This work |

In addition, $Ti_5Si_3$-15wt.% $Al_2O_3$ nanocomposite had higher fracture toughness compared to monolithic $Ti_5Si_3$. It is well known that the fracture toughness of a material not only depends on composition but also the

ability of its microstructure to dissipate deformation energy without propagation of cracks. Toughening mechanisms of crack deflection and crack bridging were suggested as important reasons for fracture toughness increase in $Ti_5Si_3$-$Al_2O_3$ nanocomposite (Fig. 6 (b)). Besides the high melting point and high hardness of $Ti_5Si_3$-$Al_2O_3$ nanocomposite, higher fracture toughness of the produced material compared to monolithic $Ti_5Si_3$ makes this nanocomposite suitable for engineering structural applications.

## 4. CONCLUSION

The Microstructure and mechanical properties of nanostructured $Ti_5Si_3$ and $Ti_5Si_3$–15wt.% $Al_2O_3$ nanocomposite was studied. Important findings are as follows:

(1) Bulk nanostructured $Ti_5Si_3$ and $Ti_5Si_3$-15wt.% $Al_2O_3$ nanocomposite were successfully fabricated by mechanical alloying and pressure-less sintering in vacuum.

(2) Amorphous/nanocrystalline microstructure was found in the $Ti_{62.5}Si_{37.5}$ powder mixture after 60h of mechanical alloying. Furthermore, in-situ produced $Al_2O_3$ reinforcements in the $Ti_5Si_3/Al_2O_3$ composite were in amorphous structure which were crystallized during sintering process.

(3) Nanohardness, elastic modulus and fracture toughness of $Ti_5Si_3$-15wt.% $Al_2O_3$ nanocomposite were determined as 1660 HV, 238 GPa and 5.5 MPa.$m^{1/2}$, respectively, which are higher than those of the monolithic $Ti_5Si_3$.

(4) Toughening mechanisms based on crack deflection and crack bridging were suggested as responsible factors for fracture toughness increase of the $Ti_5Si_3/Al_2O_3$ nanocomposite.

## REFERENCES


1. Stollof, N.S., "An overview of powder processing of silicides and their composites", ***Materials Science and Engineering A,*** Vol. 261, (1999), 169-180.
2. Koch, C.C., "Intermetallic matrix composites prepared by mechanical alloying—a review", ***Materials Science and Engineering A,*** Vol. 244, (1998), 39-48.
3. Zhang, L., Wu, J., "$Ti_5Si_3$ and $Ti_5Si_3$ – based alloys, alloying behavior, microstructure and mechanical property evaluation", ***Acta Materialia,*** Vol. 46, No. 10, (1998), 3535-3546.
4. Thadhani, N.N., Namjoshi, S., Counihan, P.J., Crawford, A., "Shock-assisted synthesis of Ti5Si3 intermetallic compound", ***Journal of Materials Processing Technology,*** Vol. 85, (1999), 74-78.
5. Yeh, C.L., Chen, W.H., Hsu, C.C., "Formation of titanium silicides $Ti_5Si_3$ and $TiSi_2$ by self propagating cumbustion synthesis", ***Journal of Alloys and Compounds,*** Vol. 432, (2007), 90-95.
6. Li, J., Jiang, D., Tan, S., "Microstructure and mechanical properties of in situ produced Ti5Si3/TiC nanocomposites", ***Journal of European Ceramic Society,*** Vol. 22, (2002), 551-558.
7. Counihan. P.J., Crawford. A., Thadhani. N.N., "Influence of dynamic densification on nanostructure formation in $Ti_5Si_3$ intermetallic alloy and its bulk properties", ***Materials Science and Engineering A,*** Vol. 267, (1999), 26-35.
8. Yazdian, N., Karimzadeh, F., Enayati, M.H., "In-situ fabrication of $Al_3V/Al_2O_3$ nanocomposite through mechanochemical synthesis and evaluation of its mechanism", ***Advanced Powder Technology,*** Vol. 24, No. 1, (2013), 106–112.
9. Williamson, K., Hall, W.H., "X-Ray line broadening from field Aluminum and Wolfram", ***Acta Metallurgica,*** Vol. 1, (1953), 22–31.
10. Oliver, W.C., Pharr, G.M., "An improved technique for determining hardness and elastic modulus using load and displacement sensing indentation experiments", ***Journal of Materials Research,*** Vol. 7, (1992), 1564-1583.
11. Sabooni, S., Karimzadeh, F., Abbasi, M.H., "Thermodynamic aspects of nanostructured Ti5Si3 formation during mechanical alloying and its characterization", ***Bulletin of Materials Science,*** Vol. 35, No. 3, (2012), 439-447.
12. Wu, J.M., "Nanosized amorphous $Al_2O_3$ particles obtained by ball milling ZnO and Al powder mixture", ***Materials Letter,*** Vol. 48, (2001), 324-330.
13. Mohammad Sharifi, E., Karimzadeh, F., Enayati, M.H., "A study on mechanochemical behavior of $B_2O_3$–Al system to produce alumina-based nanocomposite", ***Journal of Alloys and Compounds,*** Vol. 482, (2009), 110-113.
14. Jang, B.-K., Enoki, M., Kishi, T., Oh, H.-K., "Effect of second phase on mechanical properties and toughening of $Al_2O_3$ based ceramic composites", ***Composite Engineering,*** Vol. 5, No. (10-11), (1995), 1275 -1286.
15. Wang, H.Z., Gao, L., Guo, J.K., "The Effect of Nanoscale SiC Particles on the Microstructure of $Al_2O_3$ Ceramics", ***Ceramics International,*** Vol. 26, (2000), 391- 396.
16. Chang, K., Feng, W., Chen, L.Q., "Effect of second-phase particle morphology on grain growth kinetics", ***Acta Materialia,*** Vol. 57, (2009), 5229-5236.
17. Rosenkranz, R., Frommeyer, R., Smarsly, W., "Microstructure and properties of high melting point intermetallic $Ti_5Si_3$ and $TiSi_2$ compounds", ***Materials Science and Engineering A,*** Vol. 152, (1992), 288-294.
18. Cheon, Y.W., Jo, Y.J., Lee, C.M., Jang, H.S., Kim, K.B., Lee, W.H., "Consolidation of mechanically alloyed Ti-37.5at.% Si powder mixture using an electro discharge technique", ***Materials Science and Engineering A,*** Vol. 467, (2007), 89-92.
19. Quinn, G.W., Bradt, R.C., "On the Vickers indentation fracture toughness test", ***Journal of American Ceramic Society,*** Vol. 90, No. 3, (2007), 673-680.
20. Rice, R.W., Freiman, S.W., Becher, P.F., "Grain size dependence of fracture energy in ceramics: I: Experiment", ***Journal of American Ceramic Society,*** Vol. 64, (1981), 345-355.